Title
K2-66b and K2-106b: Two Extremely Hot Sub-Neptune-size Planets with High Densities

Journal
The Astronomical Journal, 153(6)

ISSN
0004-6256

Authors
Sinukoff, Evan
Howard, Andrew W
Petigura, Erik A
et al.

Publication Date
2017-06-01

DOI
10.3847/1538-3881/aa725f

Draft version May 11, 2017
Preprint typeset using LaTeX style emulateapj v. 01/23/15

K2-66B AND K2-106B: TWO EXTREMELY HOT SUB-NEPTUNE-SIZE PLANETS WITH HIGH DENSITIES

Evan Sinukoff[1,2,16] Andrew W. Howard[2], Erik A. Petigura[3,17], Benjamin J. Fulton[1,2,18], Ian J. M. Crossfield[4,19], Howard Isaacson[5], Erica Gonzales[6], Justin R. Crepp[6], John M. Brewer[7], Lea Hirsch[5], Lauren M. Weiss[8], David R. Ciardi[9], Joshua E. Schlieder[10], Bjoern Benneke[3], Jessie L. Christiansen[9], Courtney D. Dressing[3,17], Brad M. S. Hansen[11], Heather A. Knutson[3], Molly Kosiarek[4], John H. Livingston[12], Thomas P. Greene[13] Leslie A. Rogers[14] Sébastien Lépine[15]

Draft version May 11, 2017

ABSTRACT

We report precise mass and density measurements of two extremely hot sub-Neptune-size planets from the *K2* mission using radial velocities, *K2* photometry, and adaptive optics imaging. K2-66 harbors a close-in sub-Neptune-sized ($2.49^{+0.34}_{-0.24}$ $R_\oplus$) planet (K2-66b) with a mass of $21.3 \pm 3.6\,M_\oplus$. Because the star is evolving up the sub-giant branch, K2-66b receives a high level of irradiation, roughly twice the main sequence value. K2-66b may reside within the so-called "photoevaporation desert", a domain of planet size and incident flux that is almost completely devoid of planets. Its mass and radius imply that K2-66b has, at most, a meager envelope fraction ($< 5\%$) and perhaps no envelope at all, making it one of the largest planets without a significant envelope. K2-106 hosts an ultra-short-period planet ($P = 13.7$ hrs) that is one of the hottest sub-Neptune-size planets discovered to date. Its radius ($1.82^{+0.20}_{-0.14}$ $R_\oplus$) and mass ($9.0 \pm 1.6\,M_\oplus$) are consistent with a rocky composition, as are all other small ultra-short-period planets with well-measured masses. K2-106 also hosts a larger, longer-period planet ($R_p = 2.77^{+0.37}_{-0.23}$ $R_\oplus$, $P = 13.3$ days) with a mass less than 24.4 $M_\oplus$ at 99.7% confidence. K2-66b and K2-106b probe planetary physics in extreme radiation environments. Their high densities reflect the challenge of retaining a substantial gas envelope in such extreme environments.

1. INTRODUCTION

Approximately one third of Sun-like stars host planets between the size of Earth and Neptune ("sub-Neptunes") with orbital periods $P < 100$ days (Howard et al. 2012; Fressin et al. 2013; Petigura et al. 2013; Burke et al. 2015). Most sub-Neptunes detected to date were discovered by the prime *Kepler* mission (2009–2013). While *Kepler* provided a detailed measure of the distribution of planet radii, only a few tens of stars hosting sub-Neptunes were bright enough for secure mass-measurements by current generation precision radial velocity (RV) facilities (e.g. Marcy et al. 2014). Many other planets have masses measured from transit timing variations (TTVs, Holman & Murray 2005; Agol et al. 2005), a technique that is limited to compact, multiplanet systems (e.g. Carter et al. 2012; Hadden & Lithwick 2014).

Mass and radius measurements yield planet densities, which can be used to infer bulk compositions and probe planet formation histories. From the dozens of sub-Neptunes with measured densities, bulk compositional trends have become apparent. Most notably, the majority of planets smaller than $\approx 1.6\,R_\oplus$ have primarily rocky compositions, whereas most larger planets have lower densities, consistent with the presence of extended envelopes of H/He and other low-density volatiles (Weiss & Marcy 2014; Marcy et al. 2014; Rogers 2015; Dressing et al. 2015).

This overall trend in bulk compositions likely has a temperature dependence, which has yet to be fully explored. The gaseous envelopes of planets at extreme temperatures are subjected to photoevaporation by the incident radiation from their host stars (e.g. Owen & Wu 2013; Lopez & Fortney 2014). Probing planets at extreme temperatures is crucial to understand these sculpting effects and the formation histories of planets close

[1] Institute for Astronomy, University of Hawai'i at Mānoa, Honolulu, HI 96822, USA
[2] Cahill Center for Astrophysics, California Institute of Technology, 1216 East California Boulevard, Pasadena, CA 91125, USA
[3] Division of Geological and Planetary Sciences, California Institute of Technology, 1255 East California Blvd, Pasadena, CA 91125, USA
[4] Department of Astronomy & Astrophysics, University of California Santa Cruz, 1156 High St., Santa Cruz, CA, USA
[5] Astronomy Department, University of California, Berkeley, CA, USA
[6] Department of Physics, University of Notre Dame, 225 Nieuwland Science Hall, Notre Dame, IN, USA
[7] Department of Astronomy, Yale University and 260 Whitney Avenue, New Haven, CT 06511, USA
[8] Institut de Recherche sur les Exoplanètes, Dèpartement de Physique, Universitè de Montrèal, C.P. 6128, Succ. Centre-ville, Montréal, QC H3C 3J7, Canada
[9] IPAC-NExScI, Mail Code 100-22, Caltech, 1200 E. California Blvd., Pasadena, CA 91125, USA
[10] Exoplanets and Stellar Astrophysics Laboratory, NASA Goddard Space Flight Center, Greenbelt, MD 20771, USA
[11] Department of Physics & Astronomy and Institute of Geophysics & Planetary Physics, University of California Los Angeles, Los Angeles, CA 90095, USA
[12] Department of Astronomy, The University of Tokyo, 7-3-1 Bunkyo-ku, Tokyo 113-0033, Japan
[13] NASA Ames Research Center, Space Science and Astrobiology Division, M.S. 245-6, Moffett Field, CA 94035, USA
[14] Department of Astronomy & Astrophysics, University of Chicago, 5640 South Ellis Avenue, Chicago, IL 60637, USA
[15] Department of Physics and Astronomy, Georgia State University, GA, USA
[16] NSERC Postgraduate Research Fellow
[17] Hubble Fellow
[18] NSF Graduate Research Fellow
[19] NASA Sagan Fellow

to their host stars. If these planets did form as mini-Neptunes and/or giant planets, studying the masses and compositions of their remnants provides insight into the nature of the cores of such planets, specifically the mechanisms that formed them, put them so close to their host stars, and removed their surrounding envelopes.

Recent studies of planet occurrence as a function of radius and temperature have shed light on the formation and evolution of sub-Neptunes. The prime *Kepler* mission revealed that the occurrence of 2–4 $R_\oplus$ planets drops significantly at very short orbital periods ($P<$ 10 days, Howard et al. 2012; Fressin et al. 2013). Moreover, from a study of Kepler planets and planet candidates, including 157 with astroseismically characterized host stars, Lundkvist et al. (2016) reported a complete absence of planets with radii 2.2–3.8 $R_\oplus$ and incident fluxes $S_{\rm inc} >$ 650 $S_\oplus$. Evolutionary models have explained this gap as a "photoevaporation desert", because planets in this size and temperature regime have their envelopes stripped by photoevaporation (Owen & Wu 2013; Lopez & Fortney 2013). Alternatively, smaller planet cores might form too late and/or too close to the star to accrete much gas and grow in size (Lee & Chiang 2016).

Another rare sub-class of small planets are those with orbital periods $P < 1$ day, known as "ultra-short-period" planets (hereafter USPs). They exist around $\sim 1\%$ of Sun-like stars (Sanchis-Ojeda et al. 2014). While it is unclear how USPs form and how they end up so close to the star, there are several observational clues: Systems with USPs commonly host additional planets, which might have played a role in their formation and/or migration histories. Moreover, Sanchis-Ojeda et al. (2014) measured a sharp decrease in the occurrence of USPs larger than $\sim 1.4\,R_\oplus$, and a complete lack of USPs $>2.0\,R_\oplus$. Lopez (2016) showed that the observed dearth of USPs $R_p = 2$–$4\,R_\oplus$ suggests that they formed with water-poor H/He envelopes that were subsequently lost via photoevaporation.

Bulk density measurements of these two rare types of sub-Neptunes can reveal whether they are bare cores, or contain a significant amount of volatiles. Unfortunately, there have been few opportunities to study their compositions. The few of them discovered in the prime *Kepler* field orbit stars too faint for spectroscopic follow-up. However, in 2014, NASA's *K2* mission began a new chapter in the search for planets orbiting bright stars. The *Kepler* spacecraft has been collecting precise photometry of numerous fields along the ecliptic plane, each for nearly three continuous months (Howell et al. 2014). With 10,000–20,000 stars per campaign, hundreds of transiting planet candidates have been discovered (Vanderburg et al. 2015; Pope et al. 2016; Barros et al. 2016; Adams et al. 2016a), many of which have been statistically validated or confirmed as planets (Sinukoff et al. 2016; Crossfield et al. 2016). This includes several USPs around bright stars amenable to Doppler spectroscopy, including WASP-47e (Becker et al. 2015; Dai et al. 2015; Sinukoff et al. 2017) and HD 3167b (Vanderburg et al. 2016). *K2* also provides an opportunity to probe the compositions of planets in and at the boundaries of the photoevaporation desert.

Here we report the first mass and density measurements of a planet in the photoevaporation desert as well as the mass and density of a USP planet in a multi-planet system. K2-66 (EPIC 206153219) is a G1 subgiant star in *K2* Campaign 3 (C3), which hosts a transiting sub-Neptune in the photoevaporation desert. K2-106 (EPIC 220674823) is a G-star in *K2* Campaign 8 (C8) with two transiting sub-Neptunes, including a USP sub-Neptune (K2-106b). We note that K2-66b was first reported as a planet candidate by Vanderburg et al. (2015) and statistically validated by Crossfield et al. (2016). Both K2-106 planets were first reported and statistically validated by Adams et al. (2016b) as part of the Short-Period Planets Group effort (SuPerPiG).

In §2 we describe the methods by which we generate stellar light curves from raw *K2* photometry and summarize our adaptive optics imaging and Doppler observations. §3 explains our analysis of the resulting light curves, AO images, and RV time-series to precisely characterize the host stars and determine planet masses and radii. In §4, we present our results, discuss possible planet compositions, and place these planets in context with other sub-Neptunes. Concluding statements are provided in §5.

2. OBSERVATIONS

2.1. *K2 Photometry*

NASA's *Kepler* Telescope collected nearly continuous photometry of K2-66 from 2014 November 15 – 2015 January 23 UT (69 days) as part of *K2* Campaign 3. K2-106 was observed from 2016 January 04 – 2016 March 23 UT (80 days) as part of *K2* Campaign 8. We generated stellar light curves from the respective target pixel files using the same procedures detailed in Sinukoff et al. (2016) and Crossfield et al. (2016). The same Gaussian process was used to model and subtract the spacecraft motion from *K2* pixel data. We use the same K2-66 light curve presented in Crossfield et al. (2016), so we do not display it in this work.

2.2. *Adaptive Optics Imaging*

We observed K2-106 on 2016 August 24 UT with the high-contrast adaptive optics (AO) system on the Keck-II telescope using the NIRC2 imaging instrument (PI: Keith Matthews). The images were obtained in the narrow camera mode using a 3-point dither pattern with nods of 2″ in each cardinal direction to remove background light. The K_s filter was used for all observations. Conditions were foggy and the star was at airmass 1.2 with seeing of 0.″8 during the observations. Crossfield et al. (2016) presented NIRC2 adaptive optics imaging of K2-66 obtained by our group, which we do not show here. The star was found to be single. Moreover, Adams et al. (2016b) presented similar NIRC2 observations of K2-106, finding no evidence of secondary sources.

2.3. *Radial Velocity Measurements*

RV measurements of K2-66 and K2-106 were made using HIRES (Vogt et al. 1994) at the W. M. Keck Observatory. We collected 38 RV measurements of K2-66 from 2015 September 20 UT to 2017 January 07 UT and 35 RV measurements of K2-106 from 2016 August 12 UT to 2017 January 22 UT. Observations and data reduction followed the usual methods of the California Planet Search (CPS; Howard et al. 2010). An iodine cell was used for each observation as a wavelength calibrator and

TABLE 1
K2-66 Relative radial velocities, Keck-HIRES

BJD	RV [m s^{-1}]	Unc. [m s^{-1}] [a]	$S_{\rm HK}$ [b]
2457286.044784	6.58	4.19	N/A
2457580.106140	7.14	2.24	0.127
2457583.113840	-13.31	2.18	0.127
2457585.922824	3.35	2.10	0.128
2457586.022505	2.63	2.17	0.128
2457586.073226	4.15	2.20	0.127
2457587.027388	-8.39	2.06	0.129
2457588.028820	-2.36	2.07	0.128
2457595.974851	9.66	2.63	0.116
2457596.997324	-3.35	4.25	N/A
2457599.015841	-7.50	2.21	0.125
2457600.041053	-0.06	1.99	0.128
2457601.008159	5.21	2.29	0.126
2457612.841886	-8.28	2.64	0.128
2457613.983431	-16.35	2.69	0.131
2457615.860156	6.51	2.99	0.133
2457616.885444	13.79	2.84	0.130
2457622.027461	14.11	3.09	0.126
2457622.093780	-1.18	3.37	0.125
2457651.964266	2.48	2.83	0.135
2457652.025942	9.88	2.80	0.128
2457652.937923	-9.59	2.88	0.133
2457653.926554	-7.16	2.76	0.136
2457653.968022	-7.98	2.67	0.135
2457668.732792	-0.47	2.71	0.118
2457678.880082	-1.04	3.05	0.125
2457679.758736	-0.64	2.65	0.130
2457697.840632	-2.61	2.70	0.124
2457711.713727	-3.43	2.79	0.124
2457712.717828	0.82	2.66	0.127
2457713.715934	5.43	2.68	0.129
2457714.779542	-8.83	3.03	0.128
2457716.765754	2.09	2.95	0.125
2457745.716553	-15.72	2.80	0.127
2457745.763482	-24.08	5.15	N/A
2457746.704085	-1.96	2.73	0.128
2457747.720099	-6.56	2.59	0.127
2457760.710967	-6.37	3.04	0.124

[a] Uncertainties estimated from the dispersion in the radial velocity measured from 718 chunks. These uncertainties do not include "jitter" which is incorporated as a free parameter during the RV modeling ($\sigma_{\rm jit}$, Table 3).

[b] For three observations, the $S_{\rm HK}$ measurement failed due to a combination of poor seeing, scattered light, and overlapping orders at blue wavelengths. These measurements are listed as N/A.

TABLE 2
K2-106 Relative radial velocities, Keck-HIRES

BJD	RV [m s^{-1}]	Unc. [m s^{-1}] [a]	$S_{\rm HK}$
2457612.932644	-5.04	1.89	0.149
2457613.967264	-3.25	1.58	0.147
2457614.109833	-2.35	1.50	0.150
2457615.925879	-5.08	1.71	0.148
2457616.925922	-3.58	1.66	0.150
2457617.917421	4.13	1.53	0.148
2457618.926340	5.95	1.53	0.147
2457652.069904	10.72	1.53	0.143
2457653.036506	-0.86	1.64	0.139
2457668.986188	-11.42	1.72	0.137
2457671.780051	-24.84	1.94	0.150
2457672.066034	-5.93	1.66	0.152
2457672.780348	-6.86	1.69	0.153
2457672.964502	-12.31	1.61	0.153
2457697.825599	5.88	1.77	0.142
2457711.823439	-16.01	2.31	0.150
2457711.890113	-4.35	1.52	0.139
2457712.000267	1.74	1.94	0.132
2457712.760228	-0.49	1.75	0.137
2457713.803918	4.51	1.85	0.140
2457713.987377	-7.84	1.55	0.141
2457714.817690	1.62	1.57	0.136
2457714.952333	8.26	2.07	0.134
2457716.798647	1.70	1.91	0.139
2457717.971107	-7.35	2.40	0.124
2457718.905031	4.66	2.21	0.132
2457745.786321	1.55	1.80	0.144
2457746.762857	-5.93	1.74	0.135
2457747.817094	-9.04	1.83	0.134
2457761.774749	6.95	1.63	0.138
2457763.715781	-0.96	1.57	0.142
2457764.733619	2.21	1.79	0.139
2457765.800317	5.55	2.94	0.111
2457774.729422	-0.41	1.53	0.138
2457775.725113	2.53	1.65	0.138

[a] Uncertainties estimated from the dispersion in the radial velocity measured from 718 chunks. These uncertainties do not include "jitter" which is incorporated as a free parameter during the RV modeling ($\sigma_{\rm jit}$, Table 4).

point spread function (PSF) reference. The "C2" decker ($0\farcs87 \times 14''$ slit) provided spectral resolution $R \approx 55{,}000$ and allowed for the sky background to be measured and subtracted. An exposure meter was used to automatically terminate exposures after reaching a target signal-to-noise ratio (SNR) per pixel at 550 nm. Most K2-66 exposures were terminated at SNR $\approx$ 100 and typically lasted 20 min. K2-106 exposures proceeded until SNR $\approx$ 125 ($\sim$ 25 min). For each star, a single iodine-free exposure was taken at roughly twice the SNR using the "B3" decker ($0\farcs57 \times 14''$ slit). The standard CPS Doppler pipeline was used to measure RVs (Marcy & Butler 1992; Valenti et al. 1995; Butler et al. 1996; Howard et al. 2009). RV measurements are listed in Tables 1 and 2 for K2-66 and K2-106, respectively.

3. ANALYSIS

Here we describe the methods used to characterize planet host stars and to model our *K2* light curves and RV time series. Measured stellar parameters, light curve model parameters, and RV model parameters are listed in Tables 3 and 4 for K2-66 and K2-106, respectively.

3.1. *Stellar characterization*

From the iodine-free HIRES spectra, we measured the effective temperature ($T_{\rm eff}$), surface gravity ($\log g$), and metallicity ([Fe/H]) of K2-66 and K2-106, using the updated "Spectroscopy Made Easy" (SME) analysis tool described in Brewer et al. (2016). Previous comparison of SME results with astroseismic results demonstrated $\log g$ values accurate to 0.05 dex (Brewer et al. 2015). Stellar masses and radii were estimated using the `isochrones` Python package (Morton 2015), which fit our $T_{\rm eff}$, $\log g$, and [Fe/H] measurements to a grid of models from the Dartmouth Stellar Evolution Database (Dotter et al. 2008). Posteriors were sampled using the `emcee` Markov Chain Monte Carlo (MCMC) package (Foreman-Mackey et al. 2013). The adopted uncertainties on stellar mass and radius correspond to 68.3% (1σ) confidence intervals of the resulting posterior distributions. For K2-66, we measure a mass $M_\star = 1.11 \pm 0.04\,M_\odot$ and radius $R_\star = 1.67 \pm 0.12\,R_\odot$. These are consistent with the values $M_\star = 1.16 \pm 0.05\,M_\odot$, and $R_\star = 1.71 \pm 0.14\,R_\odot$ reported by Crossfield et al. (2016), who used the SpecMatch algorithm (Petigura 2015) instead of SME. For K2-106, we measure a mass of $0.92 \pm 0.03\,M_\odot$ and radius of $0.95 \pm 0.05\,R_\odot$. Adams et al. (2016b) measured $M_\star = 0.93 \pm 0.01\ M_\odot$, which is consistent with our measure-

ment, but they estimated $R_\star = 0.83 \pm 0.04\,R_\odot$, which is smaller than our measurement at the ~ 2.5-σ level (see discussion in §4.2.2).

To test for spectroscopic blends, we used the algorithm of Kolbl et al. (2015) to search for multiple sets of stellar lines. For both K2-66 and K2-106, we ruled out the possibility of companions in the $0\farcs87 \times 14''$ HIRES slit with $T_{\rm eff} = 3400$–6100 K, down to 1% contrast in V and R bands, and $\Delta RV > 10$ km s^{-1}.

The magnetic activity of each star was assessed by measuring $S_{\rm HK}$ indices using the Ca II H & K spectral lines (Isaacson & Fischer 2010). The $S_{\rm HK}$ measurements are listed in Tables 1 and 2 for K2-66 and K2-106 respectively. The median $S_{\rm HK}$ values from all spectra are 0.128 and 0.140. The measured $T_{\rm eff}$ and $S_{\rm HK}$ were converted into $\log R'_{\rm HK}$ values, a metric of the Ca II flux relative to the photospheric continuum (Middelkoop 1982; Noyes et al. 1984). We measure median $\log R'_{\rm HK}$ values of -5.27 and -5.15 dex, consistent with magnetically quiet stars from the California Planet Search (Isaacson & Fischer 2010). For comparison, the Sun ranges from $\log R'_{\rm HK} = -5.05$ dex to -4.85 dex over a typical magnetic cycle (Meunier et al. 2010).

Our NIRC2 images were processed using a standard flat-field, background subtraction, and image stacking techniques (e.g Crepp et al. 2012). Figure 1(a) displays the final reduced image and angular scale. Both raw and stacked images were examined for companion sources. A speckle to the right of the host star was ruled out as a companion as stacked images in the J-band filter showed it moving as a function of wavelength. Figure 1(b) shows the sensitivity to nearby companions. Contrast levels reach ΔK = 7.7 for separations beyond $0\farcs75$. Adams et al. (2016b) achieve similar contrast limits from K-band observations of K2-106, also with Keck/NIRC2 AO.

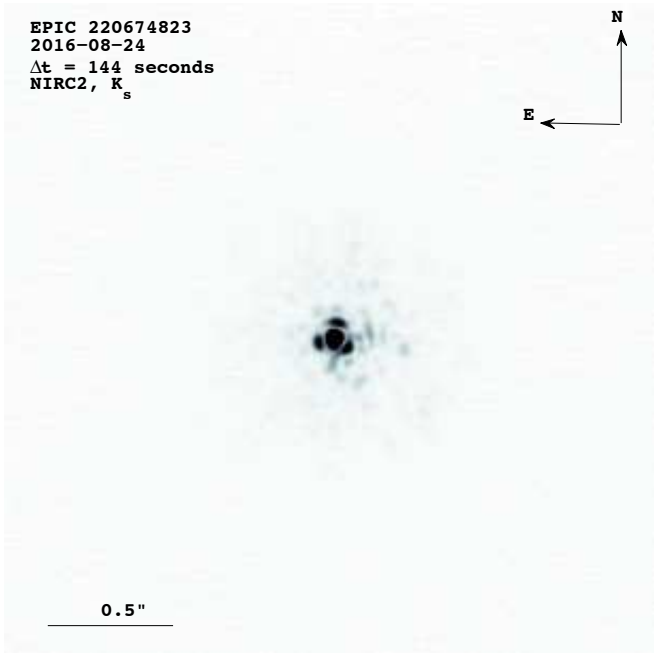

(a)

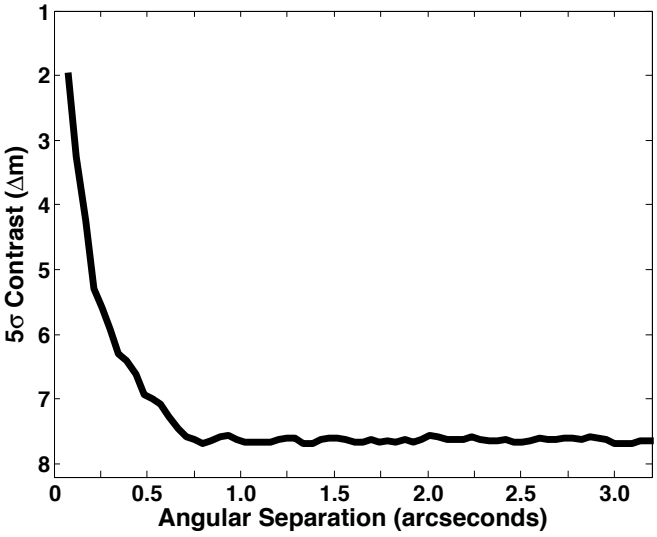

(b)

FIG. 1.— Keck/NIRC2 K_s-band adaptive optics imaging of K2-106. *(a)* Reduced image, showing no evidence of secondary stars. *(b)* 5σ contrast limits.

3.2. *Light curve analysis*

We fit transit models to the detrended K2-106 light curve using the same MCMC analysis described in Crossfield et al. (2016). In brief, our code employs the Markov Chain Monte Carlo (MCMC) package `emcee` (Foreman-Mackey et al. 2013) and model light curves are generated using the Python package `BATMAN` (Kreidberg 2015). The model parameters are: time of conjunction ($T_{\rm conj}$), orbital period, eccentricity, inclination, and longitude of periastron (P e, i, and ω), scaled semimajor axis ($a/R_\star$), ratio of planet radius to stellar radius ($R_p/R_\star$), a single multiplicative offset for the absolute flux level, and quadratic limb-darkening coefficients (u_0 and u_1). The detrended K2-106 light curve and fitted transit models for planets b and c are shown in Figure 2

3.3. *RV Analysis*

3.3.1. *Methodology*

To analyze the RV time-series of K2-66 and K2-106, we used the RV fitting package `RadVel` (B. Fulton & E. Petigura, in prep.), which is publicly available on GitHub[20]. `RadVel` is written in object-oriented Python. It uses a fast Kepler equation solver written in C and the affine-invariant sampler (Goodman & Weare 2010) of the `emcee` package (Foreman-Mackey et al. 2013). `RadVel` is easily adaptable to a variety of maximum-likelihood fitting and MCMC applications. The standard version allows for modeling of multi-planet, multi-instrument RV time-series, and assumes no interaction between planets (e.g. Sinukoff et al. 2017).

We adopt the same likelihood function for RV modeling

[20] https://github.com/California-Planet-Search/radvel
http://radvel.readthedocs.io/en/master/index.html

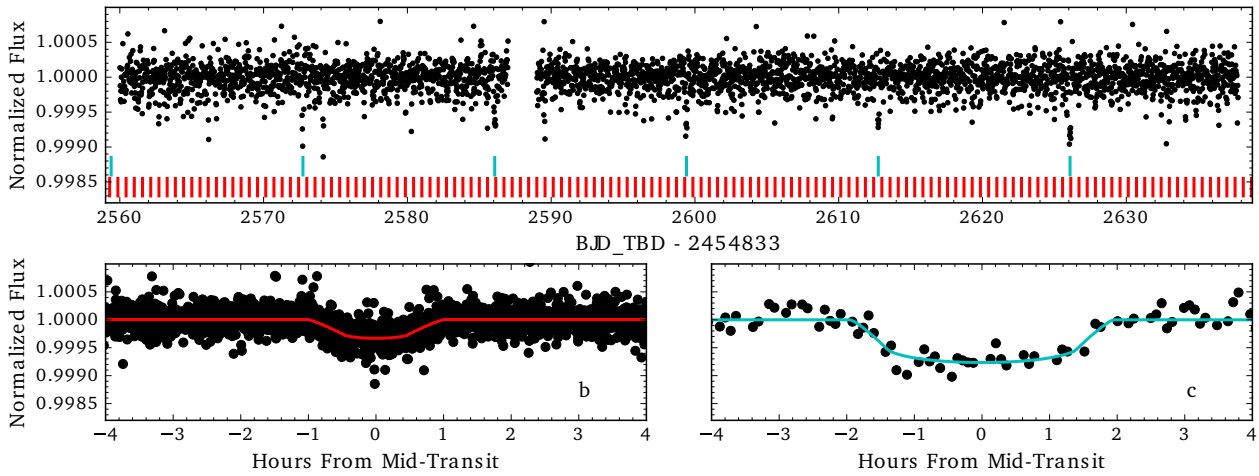

FIG. 2.— *Top*: Calibrated *K2* photometry for K2-106. Vertical ticks indicate the locations of each planets' transits. Bottom: Phase-folded photometry and best-fit light curves for each of the two planets.

as Howard et al. (2014):

$$\ln \mathcal{L} = -\sum_i \left[\frac{(v_i - v_m(t_i))^2}{2\left(\sigma_i^2 + \sigma_{\rm jit}^2\right)} + \ln \sqrt{2\pi \left(\sigma_i^2 + \sigma_{\rm jit}^2\right)} \right], \quad (1)$$

where v_i and σ_i are the ith RV measurement and corresponding uncertainty, and $v_m(t_i)$ is the Keplerian model velocity at time t_i. The same RV model parameters are used as MCMC step parameters. Before starting the MCMC exploration, we first use the minimization technique of Powell (1964) to find the maximum-likelihood model. Fifty parallel MCMC chains ("walkers") are then initialized by perturbing each of the free parameters from the maximum likelihood values by as much as 3%. An initial round of MCMC exploration continues until the Gelman-Rubin (GR) statistic (Gelman & Rubin 1992) drops below 1.10, at which point the chains are reset. Following this burn-in phase, the remaining chains are kept and the MCMC run proceeds until the GR < 1.03 and the T_z statistic (Ford 2006) exceeds 1000 for all free parameters. This ensures that the chains are well-mixed and converged.

The adopted basis for our RV model for both K2-66 and K2-106 is: $\{P,\ T_{\rm conj}\ ,\ K,\ \gamma\}$, where P is orbital period, $T_{\rm conj}$ is the time of conjunction, K is the RV semi-amplitude and γ is a constant RV offset. For K2-106, we fit for P, $T_{\rm conj}$, and K of both planets. We lock the orbital periods and phases at the photometrically measured values in Tables 3 and 4. Since the orbital ephemeris is tightly constrained from photometry, it made no difference whether we fixed the ephemeris or assigned Gaussian priors according to uncertainties on P and $T_{\rm conj}$. When testing non-circular orbits, we include two additional model parameters, $\sqrt{e}\cos\omega$ and $\sqrt{e}\sin\omega$, where e is the orbital eccentricity and ω is the longitude of periapsis of the star's orbit. This parameterization mitigates the Lucy-Sweeney bias toward non-zero eccentricity (Lucy & Sweeney 1971; Eastman et al. 2013). We also search for additional bodies at orbital periods beyond the duration of RV observations by testing RV models that include a constant acceleration term, $\mathrm{d}v/\mathrm{d}t$ (i.e. a linear trend in the RV time series). To assess whether the addition of eccentricity and constant acceleration parameters are warranted, we use the Bayesian Information Criterion (BIC). When comparing models, we lock the RV jitter at the values in Tables 3 and 4.

In §3.3.4, we discuss our search for additional planets in these two systems. We found no conclusive evidence for additional planets.

3.3.2. *K2-66*

After testing several different RV model parameterizations for K2-66, we adopt a circular orbit (sinusoidal) model with zero acceleration ($\mathrm{d}v/\mathrm{d}t \equiv 0$). The adopted RV parameters for K2-66 are listed in Table 3, including $K = 7.4 \pm 1.2\,\mathrm{m\,s^{-1}}$. The maximum likelihood RV fit is shown in Figure 3. When the orbital eccentricity is allowed to float, the MCMC fit yields $e = 0.10^{+0.13}_{-0.07}$, and a planet mass consistent with the circular orbit model. The change in the BIC is $\Delta\mathrm{BIC} = \mathrm{BIC_{ecc}} - \mathrm{BIC_{circ}} = 1.0$, which indicates that the fit does not improve enough to justify the additional free parameters (Kass & Raftery 1995). Similarly, introducing $\mathrm{d}v/\mathrm{d}t$ as a free parameter yields $\Delta\mathrm{BIC} = \mathrm{BIC}_{\mathrm{d}v/\mathrm{d}t} - \mathrm{BIC}_{\mathrm{d}v/\mathrm{d}t \equiv 0} = -0.7$, indicating no preference for the more complex model. Each of the different RV models that were tested resulted in a planet mass within 0.5σ of the adopted value.

3.3.3. *K2-106*

The adopted RV model for K2-106 is the sum of two sinusoids (two circular orbits), with $\mathrm{d}v/\mathrm{d}t \equiv 0$. The fitted RV parameters for K2-106 are listed in Table 4 and the adopted RV fit is displayed in Figure 4. Overall, the choice of model did not significantly affect the planet mass measurements — all of the RV models yielded planet mass constraints consistent with the adopted values. For planet b, we measure $K = 7.2 \pm 1.3\,\mathrm{m\,s^{-1}}$, for a 5.5σ detection. For planet c, we measure $K = 1.6 \pm 1.7\,\mathrm{m\,s^{-1}}$, which is not a reliable detection. From the posterior distribution, we place an upper limit, $K < 6.7\ \mathrm{m\,s^{-1}}$ ($M_p < 24.4\ M_\oplus$) at 99.7% confidence. Due to its proximity to the host star, the orbit of K2-106b has likely been circularized by tidal interactions with the star: We

compute a circularization timescale of ≈ 6000 years using (Goldreich & Soter 1966) assuming the same a tidal quality factor $Q = 100$ estimated for terrestrial planets in the Solar System (Goldreich & Soter 1966; Henning et al. 2009; Lainey 2016). Nevertheless, we tested a fit to the RV time series in which the eccentricity of planet b was allowed to float. The MCMC fit yielded $e = 0.11^{+0.11}_{-0.08}$, and a planet mass consistent with the best circular orbit model. Moreover, the eccentric model is not statistically favored (ΔBIC = 0.1). When the eccentricity of planet c was allowed to float, the preferred eccentricity was 0.75 and the MCMC chains did not converge. Any orbit $e \gtrsim 0.35$ would cross the stellar surface. We also ran a trial with $\mathrm{d}v/\mathrm{d}t$ as a free parameter, but found this additional model complexity was not statistically warranted (ΔBIC = 0.2). Finally, since planet c was not significantly detected, we also tried fitting for planet b alone but the measured mass changes by $< 0.5\sigma$.

There are several possible reasons why we do not detect the RV signal of planet c. One possibility is that K is sufficiently small that more data are needed to securely detect the planet. Alternatively, stellar activity on the timescale of the planet's orbital period (13 days) could partially wash out the planet signal. However, our $\log R'_{\mathrm{HK}}$ measurement of -5.15 indicates a magnetically quiet star. Finally, the star might host additional planets not included in our RV model.

3.3.4. *Search for Additional Planets*

We conducted a search for additional planets in both systems using the planet search algorithm described in Howard & Fulton (2016), which utilizes a two-dimensional Keplerian Lomb-Scargle periodogram (2DKLS, O'Toole et al. 2009). The periodogram values represent the difference in χ^2 between an N-planet model (χ^2_N) and an N+1 planet model (χ^2_{N+1}) for each orbital period value. When searching for the first planet in a given system we compare χ^2 for a 1-planet model to χ^2 for a flat line. Figure 5 shows the periodograms for $N = 0$ and $N = 1$. We estimate an empirical false alarm probability (eFAP) for any peaks in the 2DKLS periodogram by fitting a log-linear function to a histogram of periodogram values.

For K2-66, we find no evidence of additional planet signals in the RV time series. In the $N = 0$ case, the tallest peak in the periodogram occurs at 5.1 days, corresponding to the known transiting planet K2-66b. For $N = 1$, which tests the 2-planet hypothesis, the tallest peak is at $P = 4.0$ days and has eFAP $> 90\%$. We note that when we tested a 2-planet RV model with an initial period guess of 4.0 days for the second Keplerian, the measured RV semi-amplitude for K2-66b remains consistent with the adopted 1-planet model at $\approx 0.3\ \sigma$. Therefore, even if there is an additional planet at $P \approx 4$ days, it does not significantly influence our mass measurement for K2-66b.

Similarly, for K2-106, our search for additional planets in the RV time-series yields a null result. The periodogram for $N = 0$ has a global maximum at the orbital period of K2-106b (0.57 days). The $N = 1$ periodogram does not have any significant peaks — the tallest is at P = 35 days with eFAP $> 90\%$. We conclude that more RV data are needed to confidently detect any additional bodies orbiting K2-106. We note that the measured RV semi-amplitude for K2-106b changes by $< 0.5\sigma$ when a 3-planet RV model is tested with an initial period guess of 35 days for the third Keplerian. Thus, even if there is an additional planet at $P \approx 35$ days, it has a negligible effect on our mass measurement for K2-106b.

4. RESULTS & DISCUSSION

4.1. *No Significant Dilution*

Our RV detections of K2-66b and K2-106b confirm that they are bonafide planets. To verify that the planet radius measurements are accurate, we investigated the possibility that the photometric aperture contains a blend of multiple stars. Blends would dilute the transit depth, causing the planet radius to be underestimated (Ciardi et al. 2015). Figure 6 shows blend constraints from the spectroscopic analysis, AO images, and RV measurements. Together, these rule out the presence of companions that would significantly alter the measured planet radii. Contrasts in the NIRC2-AO bandpass were converted to the Kepler bandpass and to companion masses using $riJHK$ photometric calibrations of Kraus & Hillenbrand (2007). A blend with Kepler-band contrast $\Delta K_p \lesssim 2$ mag is required for a 10% error in the measured planet radius. Such companions within $\sim$ 100 AU of K2-66 or K2-106 would have been detected as a linear trend in the RV time-series and would have been detected inside $\sim$ 5 AU as secondary lines in the HIRES spectrum. AO imaging rules out problematic companions beyond $\sim$ 10 AU. We note that the plotted constraints from RV observations use Equation 1 of Winn et al. (2010), and conservatively assume dv/dt values equal to the 3-σ upper limits obtained when dv/dt is included as a free model parameter. The only conceivable problematic blend that would be undetected is a companion near apastron of a highly eccentric orbit (hence low dv/dt), at an orbital phase of low projected separation (hence undetected in AO images) and with a spectrum similar to that of the primary star (hence undetected spectral lines). However, such a scenario is highly improbable and we conclude that the likelihood of a problematic blend is negligibly low.

4.2. *Planetary Bulk Compositions*

The derived planet properties for K2-66 and K2-106 are listed in Tables 3 and 4 respectively. Figure 7(a) shows the masses and radii of K2-66b and K2-106b along with all other planets smaller than $4\,R_\oplus$, whose masses and radii are each known to better than 50% precision[21]. Here we discuss possible planet bulk compositions.

4.2.1. *K2-66*

For K2-66b, we measure a radius $R_p = 2.49^{+0.34}_{-0.24}\ R_\oplus$, and a mass $M_p = 21.3 \pm 3.6\,M_\oplus$, corresponding to bulk density $\rho_p = 7.8 \pm 2.7\,\mathrm{g\,cm^{-3}}$. It is one of the most massive planets between 2 and 3 $R_\oplus$, and likely has a massive heavy-element core. The compositions of planets in this region of the mass radius diagram are not uniquely determined and could be a range of different admixtures of various chemical species including iron, rock, water and H/He (Rogers & Seager 2010; Valencia et al. 2013).

[21] NASA Exoplanet Archive, UT 08 February 2017, http://exoplanetarchive.ipac.caltech.edu

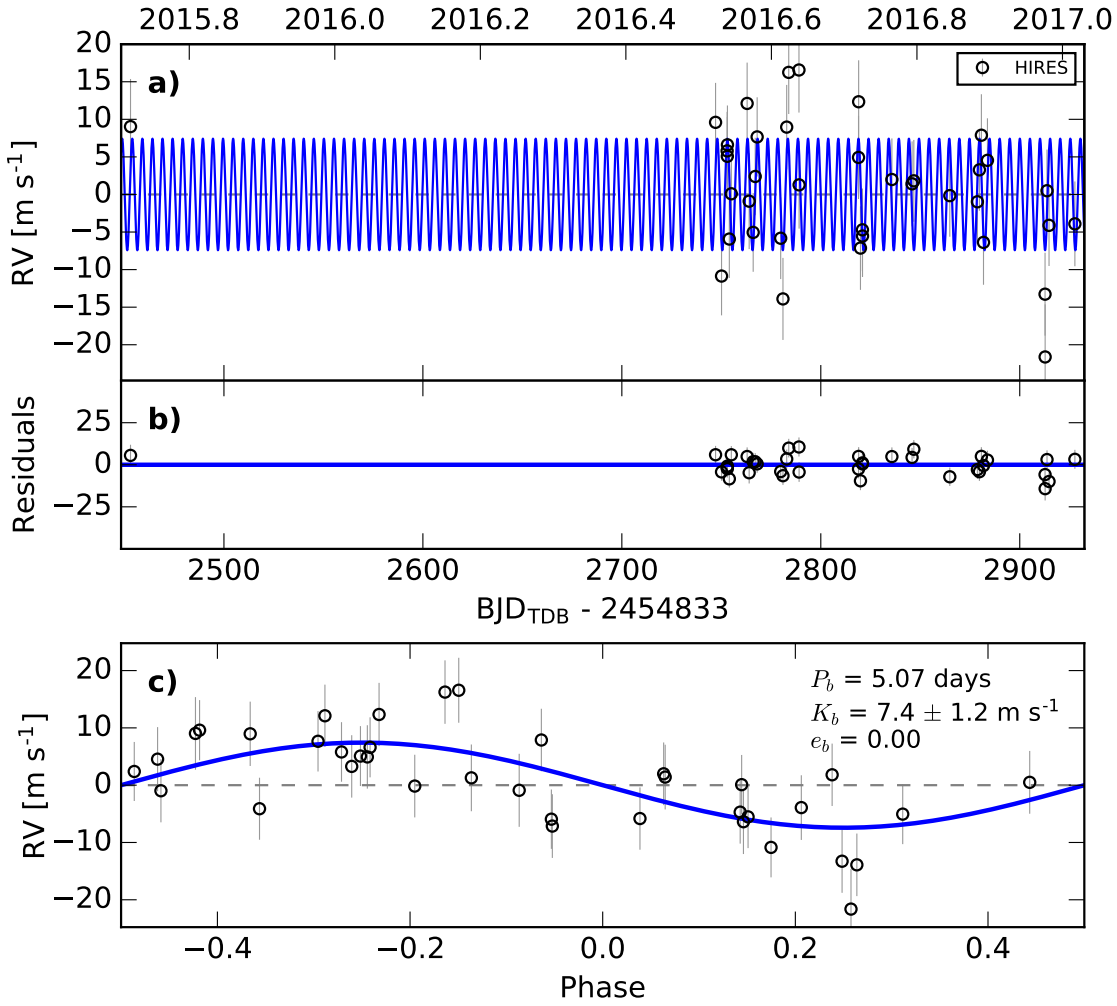

FIG. 3.— Single-planet RV model of K2-66, assuming a circular orbit and adopting the ephemeris from transit fits. *a)* The RV time-series. Open black circles indicate Keck/HIRES data. The solid blue line corresponds to the most likely model. Note that the orbital parameters listed in Table 3 are the median values of the posterior distributions. Error bars for each independent dataset include an RV jitter term listed in Table 3, which are added in quadrature to the measurement uncertainties. *b)* Residuals to the maximum-likelihood fit. *c)* The RV time-series phase folded at the orbital period of K2-66b.

To assess possible compositions, we considered a couple of different two-layer planet models and in each case we constrained the mass fraction of each layer.

First, we assumed an Earth-composition core (33% iron, 67% rock) surrounded by a solar-composition H/He envelope. We used the work of Lopez & Fortney (2014), who started with a sample of 1–20 $M_\oplus$ cores surrounded by H/He envelopes that are 0.1–50% of the total planet mass and recorded the evolution of planet radius and envelope mass over a range of incident fluxes. Their models consist of planet radii (R_p) computed over a 4-D grid of planet core mass ($M_{\rm core}$), planet envelope mass ($M_{\rm env}$), age, and incident stellar flux ($S_{\rm inc}$), i.e. $R_p = R_p$ ($M_{\rm core}$, $M_{\rm env}$, age, $S_{\rm inc}$). Following Petigura et al. (2017), we interpolated this grid to convert our measured M_p, R_p, $S_{\rm inc}$, and age into a core mass (envelope mass). We generated probability distributions for core mass fraction (CMF) by randomly sampling the posteriors of M_p, R_p, and $S_{\rm inc}$, assuming an age of 5 Gyr. Varying the age between 3–8 Gyr had negligible effect, which is explained by the fact that at Gyr ages, there is little dependence on age as the heating/cooling budget is close to a steady state value. From the resulting probability distribution, we constrain CMF > 0.96 and $M_{\rm core} > 10.8\ M_\oplus$ at 99.7% confidence (3σ). One potential limitation of our method is that the Lopez & Fortney (2014) models assume the planet incident flux is constant. However, the luminosity of K2-66 has increased by a factor of ∼2 since evolving off of the main sequence and therefore the planet incident flux was twice as low for most of its lifetime. Nevertheless, when we repeated this analysis using half the incident flux, the 3σ lower limit on the CMF changes by a negligible amount, from 0.96 to 0.95. We conclude that if the planet consists of a H/He envelope atop an Earth-composition core, the envelope is <5% of the planet's mass and the core is >10.8 $M_\oplus$. If the iron mass fraction is larger (smaller) than that of Earth, then the planet would need a more (less) extended H/He atmosphere to maintain the same radius.

We also considered a composition of rock (Mg_2SiO_4) and water ice. We randomly drew 100,000 planet masses and radii from the posterior distributions, and converted them into a rock-mass-fraction (RMF) using Equation 7 of Fortney et al. (2007). From the resulting distribution of RMFs, we conclude that if the planet is indeed a mixture of rock and water ice, then RMF > 81% at 68.3%

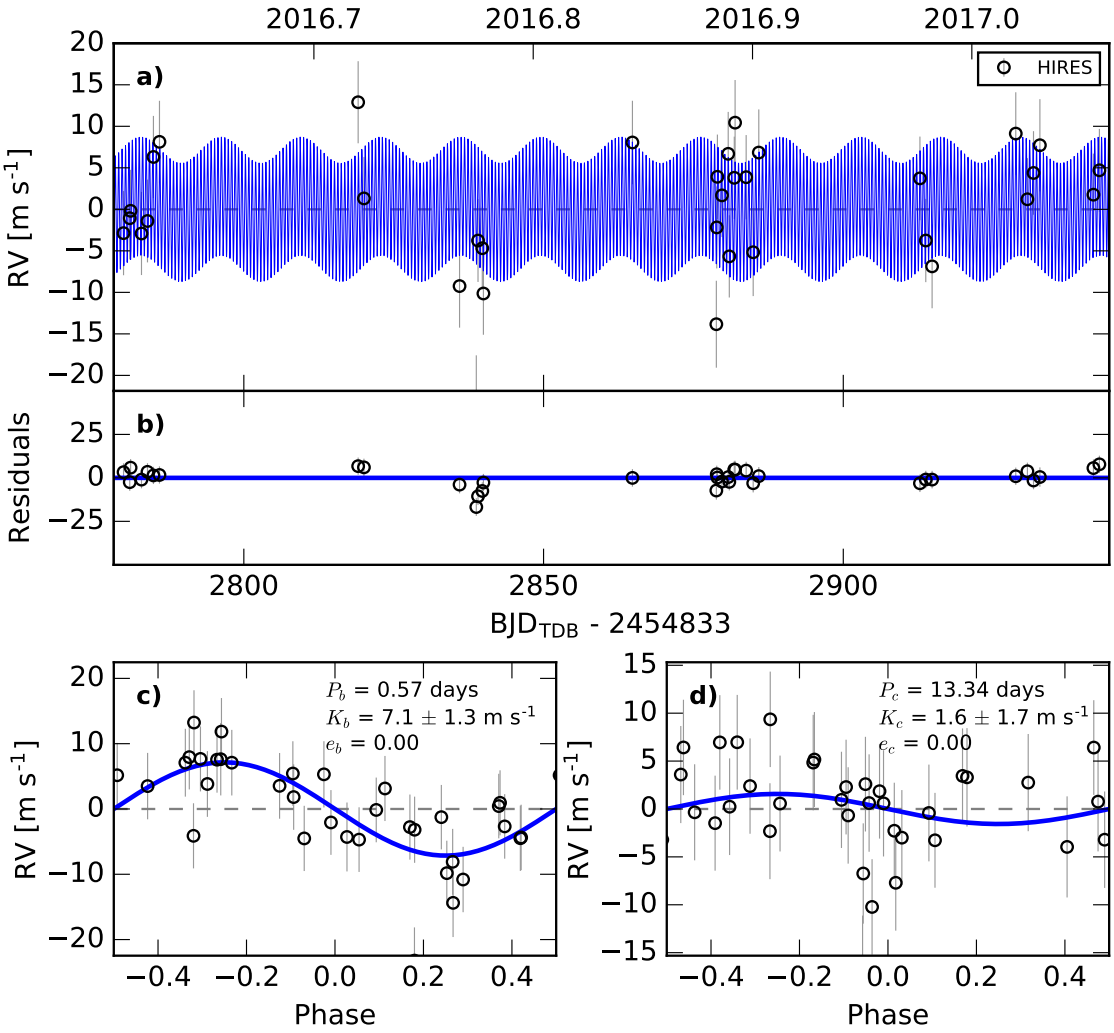

FIG. 4.— Two-planet RV model of K2-106, assuming circular orbits and adopting the ephemerides from transit fits. Details are same as Figure 3, with panels c and d showing the phase-folded light curves for planets b and c, after subtracting the signal of the other planet. We do not make a statistically significant measurement of the mass of planet c.

confidence (1σ). Moreover, the total mass of rock $M_{\rm rock}$ $> 16\,M_\oplus$ at 68.3% confidence and the planet is denser than pure rock at 39% confidence.

4.2.2. *K2-106*

For the USP planet K2-106b, we measure radius, mass, and density $R_p = 1.82^{+0.20}_{-0.14}$ $R_\oplus$, $M_p = 9.0 \pm 1.6\,M_\oplus$, and $\rho_p = 8.57^{+4.64}_{-2.80}$ g cm^{-3}. These are consistent with an Earth-like composition. Assuming the planet is a mixture of iron and rock, we used Equation 8 of Fortney et al. (2007) to convert our mass and radius posteriors into an iron mass fraction (IMF) probability distribution. The median IMF is 19% with a 1σ upper limit of 33%, consistent with an Earth-like composition. With an extremely high incident flux of $4293 \pm 483\,S_\oplus$, and equilibrium temperature of 2063 ± 58 K, K2-106b is the hottest sub-Neptune with a measured density. At such close proximity to the star, any volatiles would likely have been lost by photoevaporation, leaving a bare ~ 9 $M_\oplus$ core.

The measured radii of planets b and c are larger than those reported by Adams et al. (2016b) at the $\sim 2.5\sigma$ and $\sim 1\sigma$ level respectively. Adams et al. (2016b) measure $R_p = 1.46 \pm 0.14\,R_\oplus$ for planet b and $R_p = 2.53 \pm 0.14\,R_\oplus$ for planet c. Adopting their measured radius for planet b with our measured mass yields an iron mass fraction, IMF = 0.8 ± 0.2. Although such a large IMF is unlikely based on simulations of planet formation (e.g. Marcus et al. 2010), we investigated the source of the measurement discrepancy. We discovered that Adams et al. (2016b) underestimate the stellar radius due to an unreported error in the $T_{\rm eff}$-$R_\star$ relations of Boyajian et al. (2012), which they used to convert their spectroscopically measured $T_{\rm eff}$ (5590 ± 51 K) into a radius. Equation 8 of Boyajian et al. (2012) was reported as being a third-order polynomial fit to a sample of 33 K–M-dwarfs with precisely measured radii and $T_{\rm eff}$. Equation 9 was reported as a second polynomial fit that extends to hotter temperatures by including the Sun. However, these equations seem to have been mistakenly swapped — the polynomial coefficients in Equation 8 belong in Equation 9 and vice-versa. This can be seen by computing $R_\star$ (5778 K) = 1.00 and 0.86 $R_\odot$ for Equations 8 and 9 respectively. The two equations diverge as $T_{\rm eff}$ exceeds ~ 5300 K, which is particularly problematic. Adams et al. (2016b) used Equation 9 to compute $R_\star = 0.83$ $R_\odot$ but would have computed $R_\star = 0.91$ $R_\odot$ if they had used Equation 8, which is consistent with our measurement. Although Equation

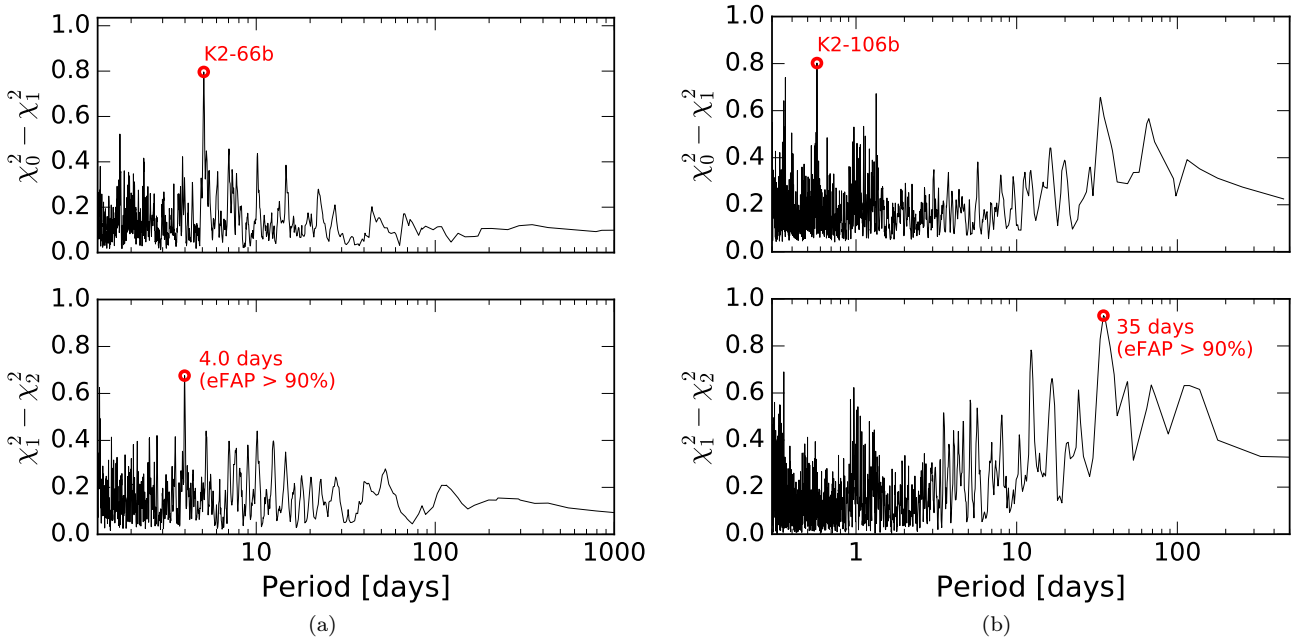

FIG. 5.— Two-dimensional Keplerian Lomb-Scargle periodograms of the measured RV time series of **a)** K2-66 and **b)** K2-106. Values on the vertical axis represent the difference in χ^2 between an N-planet model (χ^2_N) and an N+1 planet model (χ^2_{N+1}) at each period. The tallest peaks in the $N = 0$ cases (top panels) correspond to the periods of known transiting planets, as labeled. For the $N = 1$ cases (bottom panels), empirical false alarm probabilities (eFAPs) for the tallest peaks are $> 90\%$. They are likely to be spurious signals rather than the signals of additional planets.

8 is preferred for $T_{\rm eff} \gtrsim 5500\,{\rm K}$, neither are particularly reliable for this temperature regime—the Sun is the only fitted data point beyond 5500 K, which is also where $R_\star$ and $T_{\rm eff}$ become significantly age-dependent because of main sequence evolution. We encourage the authors of any studies who have used Equations 8 and 9 of Boyajian et al. (2012) to verify their results. T. Boyajian has confirmed the error and is working to publish an erratum.

We note that the $T_{\rm eff}$ and $\log g$ measured by Adams et al. (2016b) are higher than our measurements. Our spectroscopic parameters for K2-106 are derived from SME, which has been well-validated by asteroseismically characterized stars (Brewer et al. 2015). Nevertheless, even if we run the `isochrones` Python package assuming the $T_{\rm eff}$, $\log g$, and [Fe/H] values from Adams et al. (2016b), we measure stellar parameters $M_\star = 0.96\,M_\odot$ and $R_\star = 0.90\,M_\odot$, which are within our measurement errors.

4.3. *Photoevaporation Desert*

The radius and temperature of K2-66b and K2-106b constitute the extremes of planet parameter space. Figure 8 shows the radius and incident flux of confirmed planets from the NASA Exoplanet Archive[22] (NEA). K2-106b ranks among the hottest sub-Neptunes found to date. There is a clear absence of very hot planets larger than $\sim 2\,R_\oplus$. Another noticeable feature is that hotter giant planets tend to have larger radii— the reason for which is highly debated (see Ginzburg & Sari 2015, and references therein). It would be interesting to see if any trends exist for the larger sub-Neptunes of similar temperature. K2-66b occupies the region of parameter space found to be completely devoid of planets by Lundkvist et al. (2016) ($2.2\,R_\oplus < R_p < 3.8\,R_\oplus$, $S_{\rm inc} > 650\,S_\oplus$), hereafter referred to as the "L16 desert".

We find that seven other planets fall within the L16 desert. To assess the reliability of these seven measurements, we examined constraints on the host stellar parameters from spectroscopic and imaging observations. None of them were asteroseismically characterized by Lundkvist et al. (2016). According to the Exoplanet Follow-up Observing Program (ExoFOP) database[23], five of these stars (K2-100, Kepler-480, Kepler-536, Kepler-656, and Kepler-1270) have properties constrained from spectroscopy and AO imaging. One of these five stars, Kepler-536, has a stellar companion at 0.″56 separation. The planet in this system would be much larger than $4\,R_\oplus$ if it orbits the companion star rather than the primary (Law et al. 2014; Furlan et al. 2017) so we deem this measurement unreliable. We consider the planet parameters for the other four systems to be reliable and confirm that planets remain in the L16 desert when spectroscopic stellar parameters are adopted. For K2-100, we adopt the stellar and planet parameters reported in (Mann et al. 2017). The star is a late F dwarf in the 800 Myr Praesepe Cluster. For Kepler 480, Kepler-656, and Kepler-1270, we had previously obtained HIRES spectra and used the SpecMatch algorithm (Petigura 2015) to derive $T_{\rm eff}$, $\log g$, and [Fe/H]. We computed stellar masses and radii using the `isochrones` package (see §3.1). We find that Kepler-480 is an F8 dwarf, Kepler-1270 is a K1 subgiant, and K2-656 is a high-metallicity G dwarf ([Fe/H] $= 0.23 \pm 0.05$ dex). The planets in the L16 desert that orbit these four spectroscopically characterized host stars are plotted as blue

[22] NASA Exoplanet Archive, UT 15 February 2017, http://exoplanetarchive.ipac.caltech.edu

[23] https://exofop.ipac.caltech.edu/cfop.php

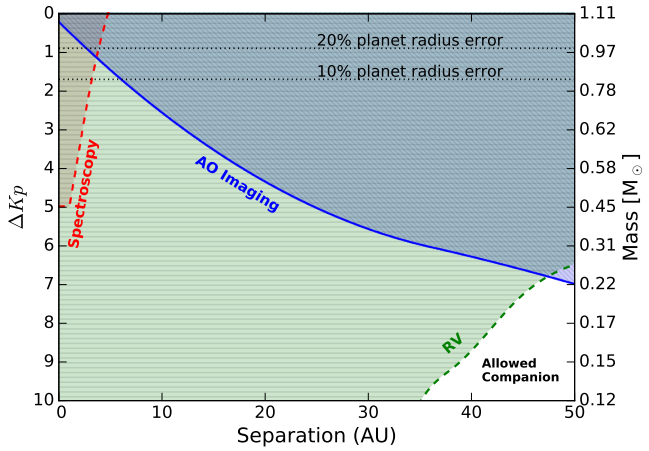

(a)

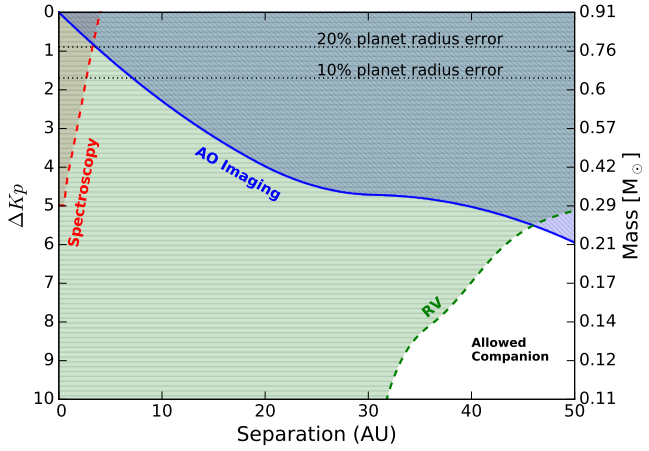

(b)

FIG. 6.— Constraints on the presence of other stars in the photometric aperture for *(a)* K2-66 and *(b)* K2-106, which would dilute the measure transit depth. The vertical axes show companion brightness contrast and companion mass plotted against orbital separation. NIRC2 AO imaging excludes companions in the hatched blue region, assuming distances of 400 pc and 250 pc to K2-66 and K2-106, respectively. The dashed red line shows the limits of our search for secondary lines in the HIRES spectrum. Companions in the hatched green region would induce a linear RV trend larger than the 3-σ upper limit determined from the RV time-series, assuming a circular, edge-on orbit. The horizontal dotted lines represent companion contrasts at which the dilution of the observed transit depths of K2-66b and K2-106b would cause planet radii to be overestimated by 10% and 20%. Together, AO imaging and spectroscopy, and RVs rule out companions that would cause systematic errors of $> 10\%$ in planet radius with high confidence (see §4.1 for discussion)

points and labeled in Figure 8.

We examine whether the five planets in the L16 desert share common properties that can be linked to their origins. First, we note that none of them are USPs — they have orbital periods of 1.3–6.0 days. Moreover, four of the five host stars have luminosities $L > 1.7\,L_\odot$. Based on these two observations, we speculate that planets in the L16 desert are 2–4 $R_\oplus$ cores of larger planets that were stripped of their gaseous envelopes by means of photoevaporation. Such 2–4 $R_\oplus$ cores would have higher surface gravities and orbit further from the star than the smaller cores of USPs. Therefore, the removal of their envelopes by photoevaporation would require stars that

TABLE 3
K2-66 SYSTEM PARAMETERS

Parameter	Value	Units
Stellar Parameters		
V	11.710 ± 0.186	mag
$T_{\rm eff}$	5887 ± 46	K
$\log g$	4.03 ± 0.05	dex
[Fe/H]	-0.047 ± 0.02	dex
$v \sin i$	3.7 ± 2.0	km s^{-1}
$M_\star$	1.11 ± 0.04	$M_\odot$
$R_\star$	1.67 ± 0.12	$R_\odot$
Planet b		
Transit Model		
P	5.06963 ± 0.00081	days
$T_{\rm conj}$	2455817.0092 ± 0.0051	BJD
$R_p/R_\star$	$0.01353^{+0.00174}_{-0.00080}$	—
$R_\star/a$	$0.127^{+0.048}_{-0.013}$	—
u_0	0.52 ± 0.01	—
u_1	0.19 ± 0.01	—
b	0.47 ± 0.31	—
i	$86.6^{+2.4}_{-4.4}$	deg
T_{14}	$4.71^{+0.45}_{-0.26}$	hrs
$\rho_{\star,\rm circ}$	$0.36^{+0.14}_{-0.22}$	g cm^{-3}
RV Model (circular orbit assumed)		
K	7.4 ± 1.2	m s^{-1}
Derived Planet Parameters		
a	0.05983 ± 0.00072	au
$S_{\rm inc}$	840 ± 125	$S_\oplus$
$T_{\rm eq}$	1372 ± 51	K
R_p	$2.49^{+0.34}_{-0.24}$	$R_\oplus$
M_p	21.3 ± 3.6	$M_\oplus$
ρ_p	7.8 ± 2.7	g cm^{-3}
Other		
γ	-2.5 ± 1.0	m s^{-1}
$\sigma_{\rm jit}$	5.0 ± 0.8	m s^{-1}

NOTE. — $S_{\rm inc}$ = incident flux, $T_{\rm conj}$ = time of conjunction. $T_{\rm eq}$ = equilibrium temperature, assuming albedo = 0.3

are systematically more luminous than USP hosts, consistent with observations. Mass measurements of other planets in the L16 desert are needed to test the hypothesis that they are cores surrounded by little to no gas.

Given that K2-66 is a subgiant star, we consider the evolution of the planet's irradiance since the star left the main sequence. According to Dartmouth stellar evolution models, a star with mass $M_\star = 1.1\,M_\odot$ and [Fe/H] = 0.05 dex would have had a radius $R_\star \approx 1.1\,R_\odot$ during its main sequence lifetime and have luminosity $L_\star \approx 1.5\,L_\odot$. Its current luminosity is $\approx 3.0\,L_\odot$, meaning that the planet incident flux has increased twofold, from ≈ 420 to $840\,S_\oplus$ since the main sequence era. This would have boosted the rate of photoevaporation of low-density volatiles in the planet's envelope. Alternatively, EPIC 206153219 might have formed in a gas-poor disk, preventing it from accumulating much H/He.

If K2-66b was stripped of its envelope as the star became a subgiant, then the rapid post-main sequence evolution explains the lack of known planets similar in size and density. Perhaps we are catching a glimpse of a planet from a population that quickly spirals into their host stars as they evolve off the main sequence (e.g.

TABLE 4
K2-106 SYSTEM PARAMETERS

Parameter	Value	Units
Stellar Parameters		
V	12.102 ± 0.212	mag
$T_{\rm eff}$	5496 ± 46	K
$\log g$	4.42 ± 0.05	dex
[Fe/H]	0.06 ± 0.03	dex
$v \sin i$	< 2.0	km s^{-1}
$M_\star$	0.92 ± 0.03	$M_\odot$
$R_\star$	0.95 ± 0.05	$R_\odot$
Planet b		
Transit Model		
P	0.571336 ± 0.000020	days
$T_{\rm conj}$	2456226.4368 ± 0.0016	BJD
$R_p/R_\star$	$0.01745^{+0.00187}_{-0.00079}$	—
$R_\star/a$	$0.366^{+0.121}_{-0.036}$	—
u_0	0.459 ± 0.001	—
u_1	0.225 ± 0.001	—
b	0.47 ± 0.32	—
i	$80.2^{+7.0}_{-12.7}$	deg
T_{14}	$1.79^{+0.56}_{-0.23}$	hrs
$\rho_{\star,\rm circ}$	$1.18^{+0.43}_{-0.68}$	g cm^{-3}
RV Model (circular orbit assumed)		
K	7.2 ± 1.3	m s^{-1}
Derived Planet Parameters		
a	0.01312 ± 0.00014	au
$S_{\rm inc}$	4293 ± 483	$S_\oplus$
$T_{\rm eq}$	2063 ± 58	K
R_p	$1.82^{+0.20}_{-0.14}$	$R_\oplus$
M_p	9.0 ± 1.6	$M_\oplus$
ρ_p	$8.57^{+4.64}_{-2.80}$	g cm^{-3}
Planet c		
Transit Model		
P	13.3387 ± 0.0018	days
$T_{\rm conj}$	2456238.7352 ± 0.0042	BJD
$R_p/R_\star$	$0.0265^{+0.0036}_{-0.0015}$	—
$R_\star/a$	$0.0368^{+0.0159}_{-0.0041}$	—
u_0	0.459 ± 0.001	—
u_1	0.225 ± 0.001	—
b	0.47 ± 0.32	—
i	$89.0^{+0.7}_{-1.4}$	deg
T_{14}	3.50 ± 0.21	hrs
$\rho_{\star,\rm circ}$	$2.13^{+0.92}_{-1.40}$	g cm^{-3}
RV Model (circular orbit assumed)		
K	1.6 ± 1.7	m s^{-1}
Derived Planet Parameters		
a	0.1071 ± 0.0015	au
$S_{\rm inc}$	64 ± 7	$S_\oplus$
$T_{\rm eq}$	722 ± 20	K
R_p	$2.77^{+0.37}_{-0.23}$	$R_\oplus$
M_p	5.7 ± 6.1	$M_\oplus$
ρ_p	1.3 ± 1.6	g cm^{-3}
Other		
γ	-2.2 ± 1.0	m s^{-1}
$\sigma_{\rm jit}$	5.1 ± 0.7	m s^{-1}

NOTE. — $S_{\rm inc}$ = incident flux, $T_{\rm conj}$ = time of conjunction. $T_{\rm eq}$ = equilibrium temperature, assuming albedo = 0.3

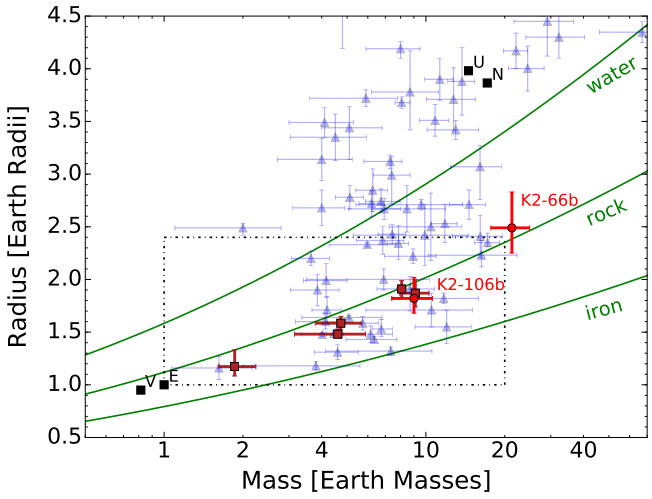

(a)

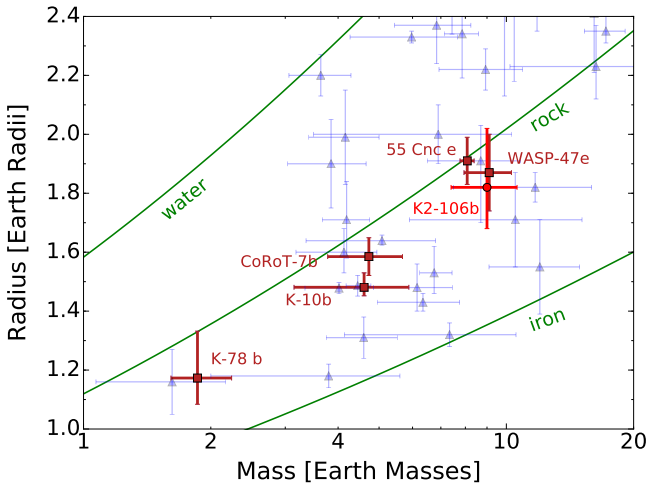

(b)

FIG. 7.— *(a)* Masses and radii of all confirmed planets whose mass and radius are measured to better than 50% (2σ) precision (blue triangles). Solar System planets are represented as black squares. Red circles indicate our measurements of K2-66b and K2-106b. Dark red squares represent other USP measurements from the literature. Green curves show the expected planet mass-radius curves for 100% iron, 100% rock (Mg_2SiO_4), and 100% water (ice) compositions according to models by Fortney et al. (2007). *(b)* A zoomed in look of the top panel. The five well-characterized USPs all have masses and radii consistent with mostly rocky compositions and little to no gaseous envelopes.

KELT-8b, Fulton et al. 2015). To test this scenario, we computed an inspiral time, $t_{\rm inspiral} \approx 370$ Gyr for K2-66b using Equation 1 of Lai (2012) assuming a nominal reduced tidal quality factor $Q'_\star = 10^7$. We conclude that the planet is not on the verge of spiraling into its host star.

4.4. *Ultra-short-period Planets*

Only five other USPs have measured masses and densities: 55 Cnc (Fischer et al. 2008; Dawson & Fabrycky 2010; Nelson et al. 2014; Demory et al. 2016), CoRoT-7b (Léger et al. 2009; Bruntt et al. 2010; Haywood et al. 2014), Kepler-10b (Batalha et al. 2011; Esteves et al. 2015), Kepler-78b (Howard et al. 2013; Pepe et al. 2013; Grunblatt et al. 2015), and WASP-47e (Becker et al.

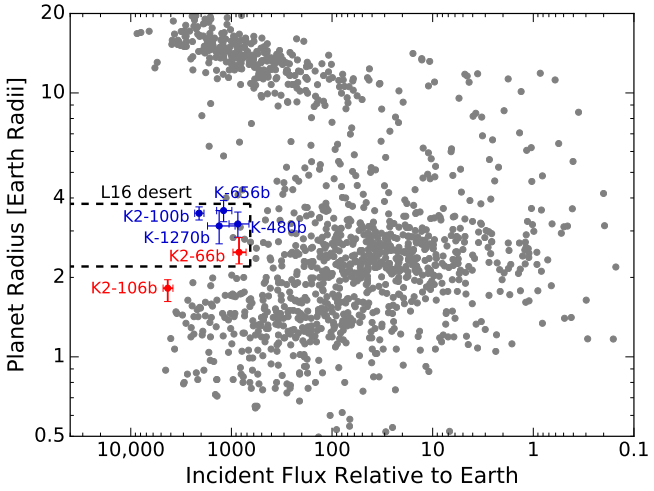

FIG. 8.— Radii and incident fluxes of all confirmed planets from the NASA Exoplanet Archive. K2-66b and K2-106b are shown in red. The black dashed box encloses the region of parameter space found by citetLundkvist16 to completely lack planets, which we refer to as the L16 desert. K2-66b, as well as three other planets (blue) occupy the L16 desert and have host stars characterized by both spectroscopic and AO observations. Four of these five planets have host stars with super-solar luminosities. K2-106b is one of the hottest sub-Neptunes found to date.

2015; Dai et al. 2015; Sinukoff et al. 2017). These planets are plotted on the mass-radius diagram in Figure 7(b). The properties of these planets and their host stars are provided in Table 5. All of them have masses and radii consistent with admixtures of rock and iron with little to no surrounding volatiles. This is consistent with the notion that USPs are the remnant cores of larger planets that lost their gaseous envelopes or formed without much gas in the first place. It is curious that three of the six well-characterized USPs have consistent masses and radii that are $\sim$ 1.7–2.0 $R_\oplus$ and $\sim$ 8–10 $M_\oplus$. Perhaps these planets constitute an upper size and mass limit to the cores of the larger planets from which they form. If all USPs have similar rocky compositions, then the observed absence of USPs >2.0 $R_\oplus$ naturally translates to an upper mass limit. Some sub-Neptune-size planets with P > 1 day have cores > 10 $M_\oplus$ (e.g. K2-66b), but there are no such examples of USPs. More well-characterized USPs are needed to reveal their core mass distribution.

We note that the three well-characterized USPs with $\sim$ 8–10 $M_\oplus$ cores (K2-106b, 55 Cnc e, WASP-47e) have host stars with super-solar metallicities, whereas two of the three well-characterized USPs with masses $\lesssim$ 5 $M_\oplus$ (Kepler-78b and Kepler-10b) have host stars with sub-solar metallicities. With only six data points, a correlation cannot be claimed, but this motivates a more complete analysis of all USPs beyond the scope of this study.

USPs are unlikely to be remnants of hot-Jupiters. While earlier studies argued that USPs could be the left-over cores of hot-Jupiters that experienced Roche lobe overflow (RLO, e.g. Valsecchi et al. 2014), simulations by Valsecchi et al. (2015) and Jackson et al. (2016) suggest that RLO of planets with cores $\lesssim$ 10 $M_\oplus$ would tend to expand their orbits to P > 1 day. Moreover, Winn et al. (2017) found that the [Fe/H] distribution of USP host stars is inconsistent with that of hot-Jupiter host stars, and consistent with that of stars hosting hot planets of Neptune-size or smaller. This suggests the that the majority of USPs are not remnants of hot-Jupiters but could be remnants of Neptune- or sub-Neptune-size planets.

Five of the six well-characterized USPs have known planetary companions. The single exception is Kepler-78b, which orbits an active star, hampering the ability to detect planets with longer orbital periods. The number of detected companions to USPs is consistent with a 50–100% occurrence rate of additional planets P < 45 days, depending on the assumed distribution of mutual inclinations and assuming 100% detection completeness (Adams et al. 2016b).

It remains unclear how USPs settle so close to their host stars, but the multiplicity of these systems (P < 50 days) hints that they form via inward migration mechanisms involving multiple planets. For example, Hansen & Zink (2015) demonstrated that tidal decay of 55 Cnc e from beyond its current orbit would have sent the planet through multiple secular resonances, exciting its orbital eccentricity and inclination. A shrinking periastron distance would subsequently boost tidal evolution and increase the rate of orbital decay. However, unless the perturber has a mass comparable to Jupiter, secular interactions are usually too weak to overcome relativistic precession at short orbital periods (Lee & Chiang 2017). Thus, secular interactions can only explain USP systems that also host close-in giant planets like 55 Cnc and WASP-47. Alternatively, USPs might have migrated through a gas disk to their current orbits via mean motion resonances (MMRs) with other planets. However, companions of USPs detected to date are not in MMR. It is possible that resonant companions were engulfed by the star or collided to form a single object. Formation of USPs via MMR would require the disk to extend very close to the star. USPs could also have been gravitationally scattered inwards by another companion, but this is difficult to reconcile with the observed presence of multiple companions on close-in orbits, which would be unstable at modest eccentricities. Lee & Chiang (2017) show that the observed USP population is consistent with in-situ formation or disk migration followed by tidal migration. Any complete theory of planet formation must account for the presence of these rocky $\sim$ 5-10 $M_\oplus$ USPs with close neighbors.

5. CONCLUSION

We have measured the masses and densities of two extremely hot sub-Neptunes, K2-66b and K2-106b. We have characterized their stellar hosts using high-resolution spectroscopy and adaptive optics imaging. The radius of K2-66b, $R_p = 2.49^{+0.34}_{-0.24}$ $R_\oplus$ measured from *K2* photometry and mass, $M_p = 21.3 \pm 3.6$ $M_\oplus$ measured from Keck-HIRES RVs are consistent with a mostly rocky composition and little to no low-density volatiles, making it one of the densest planets of its size. It is one of the few known planets in the "photoevaporation desert" (R_p = 2.2–3.8 $R_\oplus$, $S_{\rm inc} \geq 650\, S_\oplus$), and the first such planet with a measured mass. These planets tend to orbit stars more luminous than the Sun, which suggests that they might have systematically higher densities due to increased photoevaporation. The measured radius, $R_p = 1.82^{+0.20}_{-0.14}$ $R_\oplus$ and mass, $M_p = 21.3 \pm 3.6$ $M_\oplus$ of K2-106b indicate an Earth-like composition, similar to the four other USPs with measured densities. It is the hottest sub-Neptune with a measured mass, and could

TABLE 5
Ultra-short-period planets with measured masses.

Name	$M_\star$ ($M_\odot$)	$R_\star$ ($R_\odot$)	[Fe/H] (dex)	P (days)	R_p ($R_\oplus$)	M_p ($M_\oplus$)	ρ_p (g cm^{-3})	$N_{\rm pl}$	References
55 Cnc e	0.905 ± 0.015	0.943 ± 0.010	0.31 ± 0.04	0.74	1.92 ± 0.08	8.08 ± 0.31	$6.3^{+0.8}_{-0.7}$	5	V05, V11, D16
CoRot-7b	0.91 ± 0.03	0.82 ± 0.04	0.12 ± 0.06	0.85	1.585 ± 0.064	4.73 ± 0.95	6.61 ± 1.33	2	L09, B10, H14
Kepler-10b	0.913 ± 0.022	1.065 ± 0.009	-0.15 ± 0.04	0.84	$1.48^{+0.05}_{-0.03}$	$4.61^{+1.27}_{-1.46}$	8.0 ± 3.0	2	B11, E15
Kepler-78b	0.83 ± 0.05	0.74 ± 0.05	-0.08 ± 0.04	0.36	$1.18^{+0.16}_{-0.09}$	$1.86^{+0.38}_{-0.25}$	$5.57^{+3.02}_{-1.31}$	1	S13, H13, P13
WASP-47e	0.99 ± 0.05	1.18 ± 0.08	0.36 ± 0.05	0.79	1.87 ± 0.13	9.11 ± 1.17	7.63 ± 1.90	4	B15, S17
K2-106b	0.95 ± 0.05	0.92 ± 0.03	0.06 ± 0.03	0.57	$1.82^{+0.20}_{-0.14}$	9.0 ± 1.6	$8.57^{+4.64}_{-2.80}$	2	This study

Note. — V05: Valenti & Fischer (2005), V11: von Braun et al. (2011), D16: Demory et al. (2016), L09: Léger et al. (2009), B10: Bruntt et al. (2010), H14: Haywood et al. (2014), B11: Batalha et al. (2011), E15: Esteves et al. (2015), S13: Sanchis-Ojeda et al. (2013), H13: Howard et al. (2013), P13: Pepe et al. (2013), B15: Becker et al. (2015), S17: Sinukoff et al. (2017).

be the stripped core of a more massive planet. K2-66b and K2-106b join the rare class of planets larger than 1.5 $R_\oplus$ with mostly rocky compositions.

We thank the many observers who contributed to the measurements reported here. We gratefully acknowledge the efforts and dedication of the Keck Observatory staff. We thank Tabetha Boyajian for helpful discussions. This paper includes data collected by the *K2* mission. Funding for the *K2* mission is provided by the NASA Science Mission directorate. E. S. is supported by a postgraduate scholarship from the Natural Sciences and Engineering Research Council of Canada. E. A. P. acknowledges support by NASA through a Hubble Fellowship grant awarded by the Space Telescope Science Institute, which is operated by the Association of Universities for Research in Astronomy, Inc., for NASA, under contract NAS 5-26555. B. J. F. was supported by the National Science Foundation Graduate Research Fellowship under grant No. 2014184874. A. W. H. acknowledges support for our *K2* team through a NASA Astrophysics Data Analysis Program grant. A. W. H. and I. J. M. C. acknowledge support from the *K2* Guest Observer Program. L. M. W. acknowledges the Trottier Family Foundation for their generous support. J. R. C. acknowledges support from the Kepler Participating Scientist program (NNX14AB85G). This work was performed [in part] under contract with the Jet Propulsion Laboratory (JPL) funded by NASA through the Sagan Fellowship Program executed by the NASA Exoplanet Science Institute. This research has made use of the NASA Exoplanet Archive, which is operated by the California Institute of Technology, under contract with the National Aeronautics and Space Administration under the Exoplanet Exploration Program. Finally, the authors extend special thanks to those of Hawai'ian ancestry on whose sacred mountain of Maunakea we are privileged to be guests. Without their generous hospitality, the Keck observations presented herein would not have been possible.

Facilities: Kepler, Keck-HIRES.

REFERENCES

Adams, E. R., Jackson, B., & Endl, M. 2016a, AJ, 152, 47
Adams, E. R., Jackson, B., Endl, M., et al. 2016b, ArXiv e-prints, arXiv:1611.00397
Agol, E., Steffen, J., Sari, R., & Clarkson, W. 2005, MNRAS, 359, 567
Barros, S. C. C., Demangeon, O., & Deleuil, M. 2016, A&A, 594, A100
Batalha, N. M., Borucki, W. J., Bryson, S. T., et al. 2011, ApJ, 729, 27
Becker, J. C., Vanderburg, A., Adams, F. C., Rappaport, S. A., & Schwengeler, H. M. 2015, ApJ, 812, L18
Boyajian, T. S., von Braun, K., van Belle, G., et al. 2012, ApJ, 757, 112
Brewer, J. M., Fischer, D. A., Basu, S., Valenti, J. A., & Piskunov, N. 2015, ApJ, 805, 126
Brewer, J. M., Fischer, D. A., Valenti, J. A., & Piskunov, N. 2016, ApJS, 225, 32
Bruntt, H., Deleuil, M., Fridlund, M., et al. 2010, A&A, 519, A51
Burke, C. J., Christiansen, J. L., Mullally, F., et al. 2015, ApJ, 809, 8
Butler, R. P., Marcy, G. W., Williams, E., et al. 1996, PASP, 108, 500
Carter, J. A., Agol, E., Chaplin, W. J., et al. 2012, Science, 337, 556
Ciardi, D. R., Beichman, C. A., Horch, E. P., & Howell, S. B. 2015, ApJ, 805, 16
Crepp, J. R., Johnson, J. A., Howard, A. W., et al. 2012, ApJ, 761, 39
Crossfield, I. J. M., Ciardi, D. R., Petigura, E. A., et al. 2016, ApJS, 226, 7
Dai, F., Winn, J. N., Arriagada, P., et al. 2015, ApJ, 813, L9
Dawson, R. I., & Fabrycky, D. C. 2010, ApJ, 722, 937
Demory, B.-O., Gillon, M., Madhusudhan, N., & Queloz, D. 2016, MNRAS, 455, 2018
Dotter, A., Chaboyer, B., Jevremović, D., et al. 2008, ApJS, 178, 89
Dressing, C. D., Charbonneau, D., Dumusque, X., et al. 2015, ApJ, 800, 135
Eastman, J., Gaudi, B. S., & Agol, E. 2013, PASP, 125, 83
Esteves, L. J., De Mooij, E. J. W., & Jayawardhana, R. 2015, ApJ, 804, 150
Fischer, D. A., Marcy, G. W., Butler, R. P., et al. 2008, ApJ, 675, 790
Ford, E. B. 2006, ApJ, 642, 505
Foreman-Mackey, D., Hogg, D. W., Lang, D., & Goodman, J. 2013, PASP, 125, 306
Fortney, J. J., Marley, M. S., & Barnes, J. W. 2007, ApJ, 659, 1661
Fressin, F., Torres, G., Charbonneau, D., et al. 2013, ApJ, 766, 81
Fulton, B. J., Collins, K. A., Gaudi, B. S., et al. 2015, ApJ, 810, 30
Furlan, E., Ciardi, D. R., Everett, M. E., et al. 2017, AJ, 153, 71
Gelman, A., & Rubin, D. B. 1992, Statist. Sci., 7, 457
Ginzburg, S., & Sari, R. 2015, ApJ, 803, 111
Goldreich, P., & Soter, S. 1966, Icarus, 5, 375
Goodman, J., & Weare, J. 2010, Communications in Applied Mathematics and Computational Science, 5, 65
Grunblatt, S. K., Howard, A. W., & Haywood, R. D. 2015, arXiv:1501.00369, arXiv:1501.00369
Hadden, S., & Lithwick, Y. 2014, ApJ, 787, 80
Hansen, B. M. S., & Zink, J. 2015, MNRAS, 450, 4505

Haywood, R. D., Collier Cameron, A., Queloz, D., et al. 2014, MNRAS, 443, 2517
Henning, W. G., O'Connell, R. J., & Sasselov, D. D. 2009, ApJ, 707, 1000
Holman, M. J., & Murray, N. W. 2005, Science, 307, 1288
Howard, A. W., & Fulton, B. J. 2016, PASP, 128, 114401
Howard, A. W., Johnson, J. A., Marcy, G. W., et al. 2009, ApJ, 696, 75
—. 2010, ApJ, 721, 1467
Howard, A. W., Marcy, G. W., Bryson, S. T., et al. 2012, ApJS, 201, 15
Howard, A. W., Sanchis-Ojeda, R., Marcy, G. W., et al. 2013, Nature, 503, 381
Howard, A. W., Marcy, G. W., Fischer, D. A., et al. 2014, ApJ, 794, 51
Howell, S. B., Sobeck, C., Haas, M., et al. 2014, PASP, 126, 398
Isaacson, H., & Fischer, D. 2010, ApJ, 725, 875
Jackson, B., Jensen, E., Peacock, S., Arras, P., & Penev, K. 2016, Celestial Mechanics and Dynamical Astronomy, 126, 227
Kass, R. E., & Raftery, A. E. 1995, Journal of the American Statistical Association, 90, 773
Kolbl, R., Marcy, G. W., Isaacson, H., & Howard, A. W. 2015, AJ, 149, 18
Kraus, A. L., & Hillenbrand, L. A. 2007, AJ, 134, 2340
Kreidberg, L. 2015, PASP, 127, 1161
Lai, D. 2012, MNRAS, 423, 486
Lainey, V. 2016, Celestial Mechanics and Dynamical Astronomy, 126, 145
Law, N. M., Morton, T., Baranec, C., et al. 2014, ApJ, 791, 35
Lee, E. J., & Chiang, E. 2016, ApJ, 817, 90
—. 2017, ArXiv e-prints, arXiv:1702.08461
Léger, A., Rouan, D., Schneider, J., et al. 2009, A&A, 506, 287
Lopez, E. D. 2016, arXiv:1610.01170, arXiv:1610.01170
Lopez, E. D., & Fortney, J. J. 2013, ApJ, 776, 2
—. 2014, ApJ, 792, 1
Lucy, L. B., & Sweeney, M. A. 1971, AJ, 76, 544
Lundkvist, M. S., Kjeldsen, H., Albrecht, S., et al. 2016, Nature Communications, 7, 11201
Mann, A. W., Gaidos, E., Vanderburg, A., et al. 2017, AJ, 153, 64
Marcus, R. A., Sasselov, D., Hernquist, L., & Stewart, S. T. 2010, ApJ, 712, L73
Marcy, G. W., & Butler, R. P. 1992, PASP, 104, 270
Marcy, G. W., Isaacson, H., Howard, A. W., et al. 2014, ApJS, 210, 20
Meunier, N., Desort, M., & Lagrange, A.-M. 2010, A&A, 512, A39
Middelkoop, F. 1982, A&A, 107, 31
Morton, T. D. 2015, isochrones: Stellar model grid package, Astrophysics Source Code Library, ascl:1503.010
Nelson, B. E., Ford, E. B., Wright, J. T., et al. 2014, MNRAS, 441, 442
Noyes, R. W., Hartmann, L. W., Baliunas, S. L., Duncan, D. K., & Vaughan, A. H. 1984, ApJ, 279, 763
O'Toole, S. J., Tinney, C. G., Jones, H. R. A., et al. 2009, MNRAS, 392, 641
Owen, J. E., & Wu, Y. 2013, ApJ, 775, 105
Pepe, F., Cameron, A. C., Latham, D. W., et al. 2013, Nature, 503, 377
Petigura, E. A. 2015, PhD thesis, University of California, Berkeley, arXiv:1510.03902
Petigura, E. A., Marcy, G. W., & Howard, A. W. 2013, ApJ, 770, 69
Petigura, E. A., Sinukoff, E., Lopez, E., et al. 2017, ArXiv e-prints, arXiv:1702.00013
Pope, B. J. S., Parviainen, H., & Aigrain, S. 2016, MNRAS, 461, 3399
Powell, M. J. D. 1964, The Computer Journal, 7, 155
Rogers, L. A. 2015, ApJ, 801, 41
Rogers, L. A., & Seager, S. 2010, ApJ, 712, 974
Sanchis-Ojeda, R., Rappaport, S., Winn, J. N., et al. 2014, ApJ, 787, 47
—. 2013, ApJ, 774, 54
Sinukoff, E., Howard, A. W., Petigura, E. A., et al. 2016, ApJ, 827, 78
—. 2017, AJ, 153, 70
Valencia, D., Guillot, T., Parmentier, V., & Freedman, R. S. 2013, ApJ, 775, 10
Valenti, J. A., Butler, R. P., & Marcy, G. W. 1995, PASP, 107, 966
Valenti, J. A., & Fischer, D. A. 2005, ApJS, 159, 141
Valsecchi, F., Rappaport, S., Rasio, F. A., Marchant, P., & Rogers, L. A. 2015, ApJ, 813, 101
Valsecchi, F., Rasio, F. A., & Steffen, J. H. 2014, ApJ, 793, L3
Vanderburg, A., Montet, B. T., Johnson, J. A., et al. 2015, ApJ, 800, 59
Vanderburg, A., Bieryla, A., Duev, D. A., et al. 2016, ApJ, 829, L9
Vogt, S. S., Allen, S. L., Bigelow, B. C., et al. 1994, in Society of Photo-Optical Instrumentation Engineers (SPIE) Conference Series, Vol. 2198, Instrumentation in Astronomy VIII, ed. D. L. Crawford & E. R. Craine, 362
von Braun, K., Boyajian, T. S., ten Brummelaar, T. A., et al. 2011, ApJ, 740, 49
Weiss, L. M., & Marcy, G. W. 2014, ApJ, 783, L6
Winn, J. N., Sanchis-Ojeda, R., Rogers, L., et al. 2017, arXiv:1704.00203
Winn, J. N., Johnson, J. A., Howard, A. W., et al. 2010, ApJ, 718, 575